

21C.4 CSU-CHILL RADAR OBSERVATIONS OF BRAGG SCATTERING ECHOES IN MOUNTAIN WAVE LEE FLOW.

Patrick C. Kennedy*, Steven A. Rutledge, and Russ S. Schumacher

Colorado State University Department of Atmospheric Science

Fort Collins, Colorado

1. INTRODUCTION

While weather radars are generally designed to detect the backscattered signals from hydrometeors, Bragg scattering echoes due local spatial variations in the microwave refractive index are also observed. For Bragg scattering within the inertial subrange of turbulence, the Bragg backscattering cross section is related to the magnitude of the atmospheric refractive index variations on a space scale equal to one half of the radar wavelength (Knight and Miller, 1993):

$$\eta = 0.38 C_n^2 \lambda^{-1/3} \quad (1)$$

Where:

η is the backscattering cross section per unit volume (m^2/m^3)

C_n^2 is a structure constant, expressing the magnitude of the refractive index variations on the length scale of $\frac{1}{2}$ the radar wavelength ($\text{m}^{-2/3}$)

λ is the wavelength of the observing radar (m)

In addition to radar wavelength, the refractive index embodied in C_n^2 is a function of atmospheric pressure, temperature, and water vapor content.

Two common manifestations of Bragg scattering are “inverted cup” echoes around the outer edges of cumulus clouds (Knight and Miller, 1993), and elevated, horizontal layers (Melnikov et al., 2011, Davison et al., 2013). In both cases, the Bragg echoes are quite weak, with S-band reflectivities typically on the order of -10 dBZ or less. Furthermore, Bragg echoes are ~ 19 dB weaker at X-band vs. S-band (Knight and Miller, 1993). Especially in the lower half of the troposphere, local fluctuations in water vapor content are generally more significant than temperature variations in enhancing C_n^2 (Davison et al., 2013)

The horizontal moisture stratifications associated with Bragg echo layers can become perturbed in the lee waves that develop in the vertical plane downstream of mountainous terrain under suitable vertical profiles of wind speed and thermodynamic stability. Under these conditions, the Bragg echo layer(s) can assume wave-like shapes that trace the lee wave flow (Fig. 1).

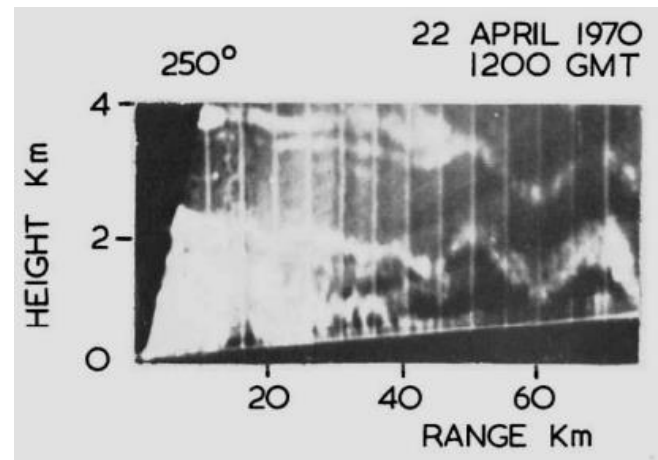


Figure 1: Analogue presentation of received signal power in an RHI scan. Bragg echo layers perturbed by lee wave airflow are observed downstream of hilly terrain in Wales. Reproduced from Figure 10 in Starr and Browning, 1972.

This paper presents observations collected by the 11 cm wavelength CSU-CHILL radar on 9 January 2017 when an episode of high surface winds and mountain wave activity was affecting much of the area immediately east of the Rocky Mountains in Colorado. The Bragg echoes detected by the radar captured the end of the relatively stable lee wave period as well as the transition to a less stable, more turbulent flow regime. The Bragg echo evolution showed good correspondence with the flow field predicted by the Weather Research and Forecasting (WRF) model.

2. OVERVIEW OF THE 9 JANUARY 2017 HIGH WIND EVENT.

Figure 2 shows the area in which high surface winds occurred. The color fill in Fig. 2 depicts the terrain elevations in km above sea level. The maximum terrain heights of 3.5 to 4 km MSL occur along the continental divide, located ~ 90 km to the west of the CSU-CHILL radar site. The radar is located in the Platte River valley at an elevation of 1.4 km MSL. The distinctly elevated terrain of the Rocky Mountains promotes the development of lee waves over the lower elevations to the east when westerly winds force stable air over the mountains.

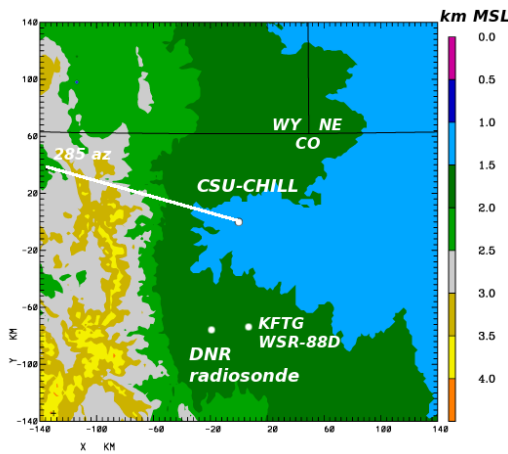


Figure 2: Terrain heights in km MSL in the vicinity of the CSU-CHILL radar. Axes are X and Y in km from the radar site. Solid white line marks the 285 degree RHI azimuth.

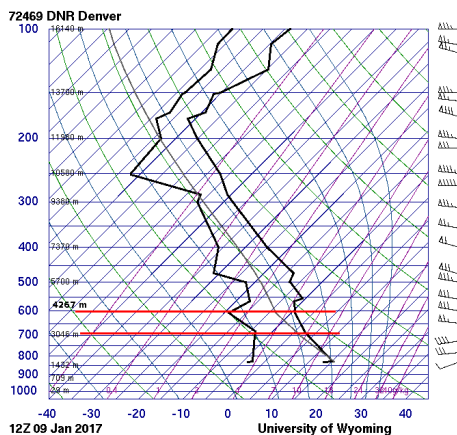


Figure 3: Skew T – log p plot of the Denver NWS sounding at 12 UTC on 9 January 2017. (See Fig. 1 for the location of DNR). Wind speeds are in knots. Red lines mark the stable layer associated with the lee wave echoes.

The NWS sounding taken at Denver shows some key aspects of the synoptic conditions at 12 UTC on 9 January 2017 (Fig. 3). The winds were generally westerly throughout the sounding, with speeds in excess of 25 ms^{-1} (50 knots) at all levels above ~650 hPa. Saturation did not exist at any height (clouds did develop over the mountains later in the day). The two highlighted levels marked on the sounding identify a stable layer within which humidity decreases with height, a configuration that has been found to promote the development of Bragg echo layers (Davison et al., 2013). Wind speeds also increase with height in this layer; this is a significant factor in the development and maintenance of lee waves (Scorer, 1949). The Denver forecast office on the National Weather Service issued a high wind warning for much of the area during on 9 January. This warning verified with surface wind gust reports of up to 44 ms^{-1} (100 mi hr^{-1}) and widespread damage to trees, power lines, etc.

3. Radar observations and WRF model results

CSU-CHILL radar operations on 9 January 2017 began at ~2100 UTC. The radar was brought up to test the operation of the liquid cooling systems that are used with the Klystron main power amplifier tubes in the horizontal and vertical polarization transmitters. Some of the radar test operations included RHI scans done on azimuths oriented towards the mountainous terrain to the west of the radar. Wave echo patterns were immediately apparent in these RHI scans. Figure 4a shows the wave echo in the reflectivity field of an RHI scan at 2110 UTC. Due to the weak echo intensity, the wave echo became difficult to detect beyond ~40 km range. The reflectivity levels were generally below -10 dBZ (yellow on the color scale). The wave pattern was more evident in the unthresholded radial velocity data (Fig. 4b). The wave echo was located below ~2.5 km AGL (3.9 km MSL); generally within the stable layer marked in Figure 2. Also in agreement with the sounding, radial velocities increased with height, with aliasing (purple to yellow color transition) evident where radial velocities exceeded 27.5 ms^{-1} .

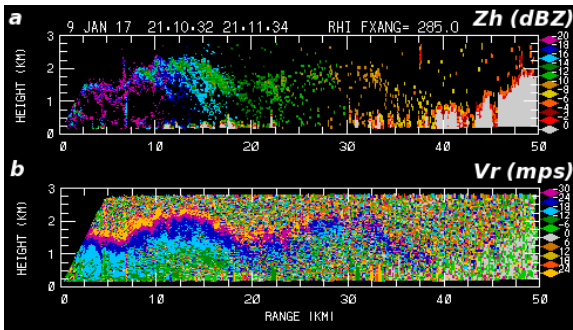


Figure 4a: Reflectivity data in the 285° RHI scan at 2110 UTC. White (> 0 dBZ) echo areas starting at 40 km range are ground returns from the eastern foothills of the Rocky Mountains. 4b: Corresponding radial velocity data

Middle and high level clouds were visible above the CSU-CHILL radar during the data collection period. The ceilometer data from the Automated Weather Observing System (AWOS) installation at the Greeley-Weld County Airport (KGXY; located ~2 km from CSU-CHILL) did not report any clouds below 3.76 km AGL (12 kft). The wave echo was essentially below the detection limit of the CSU-CHILL X-band channel. In the very few near-range gates where above-noise level X-band returns were received, the X-band reflectivity was ~ 14 dB below the corresponding S-band values. Based on the absence of ceilometer returns from the wave echo heights, and the significantly lower X-band vs. S-band reflectivity levels, it is believed that Bragg scattering (vs. returns from cloud particles or hydrometeors) was primarily responsible for the wave echo layer that was detected at S-band.

To examine the environment in which this wave echo developed, the Weather Research and Forecasting (WRF) numerical forecast model was run. In the region of interest, the model used a high-resolution sub-grid with a horizontal grid size of 1.33 km and 75 vertical levels with a near-surface spacing of ~150 m (Fig. 5). The model run was initialized at 00 UTC on 9 January 2017 to allow better stabilization of the forecast fields by the start of the CSU-CHILL observations at 21 UTC.

Figure 6 shows a vertical cross section of the model output at 2050 UTC. The cross section depicts a plane oriented west to east through the radar site, with the radar being located at X = 144 km. The air motions are generally traced by the potential temperature contour lines. A train of dampening lee waves is apparent downstream of the high terrain. Vertical velocity magnitudes of +/- 5 ms⁻¹ were diagnosed in these waves.

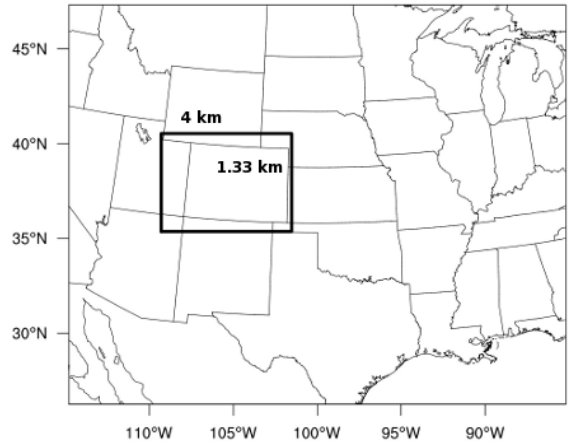


Figure 5: Horizontal domain of the WRF model. Inset box marks the higher horizontal resolution (1.33 km) interior grid centered over Colorado.

Init: 0000 UTC Mon 09 Jan 17 Valid: 2050 UTC Mon 09 Jan 17 (1350 MST Mon 09 Jan 17) Fcst: 20.83 h
 Vertical velocity XY= 302.0,333.0 to 455.0,333.0
 Potential temperature XY= 302.0,333.0 to 455.0,333.0

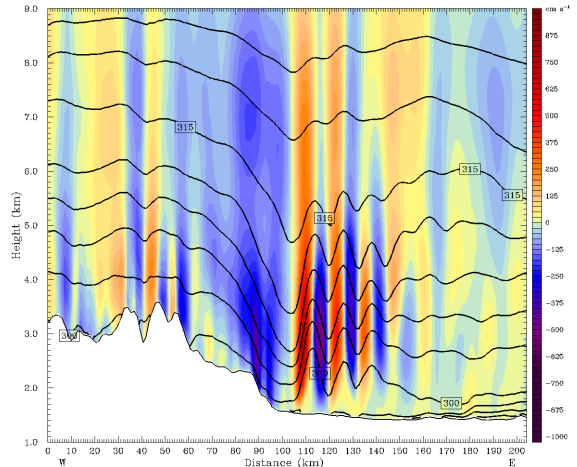


Figure 6: Vertical cross section of WRF model output at 2050 UTC. The plane is oriented west to east through the CSU-CHILL radar site (located at X=144 km). Color fill is vertical air motion in cm s⁻¹. Solid lines are potential temperature (°K).

A comparison of WRF output at 2130 UTC with the RHI scan at 2110 UTC is shown in Figure 7. In this figure the model output has been re-plotted to match the RHI orientation (i.e., west towards the right) and adjusted vertically to match the AGL height scaling of the RHI. The location and amplitude of the lee wave diagnosed by the WRF show remarkable agreement with the observed Bragg echo configuration. The model forecast wind speeds are also consistent with the development of aliasing in the radial velocities. This radar echo – model output

correspondence implies that the WRF has accurately forecast the mesoscale conditions under which the lee waves occurred.

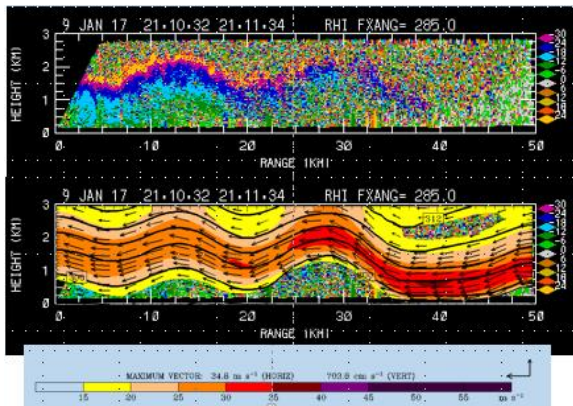


Figure 7 top: CSU-CHILL radial velocities at 2110 UTC. Bottom: Overlay of WRF wind field (vectors and color fill) and potential temperature (solid contours) at the 2130 UTC.

Several hours later at 2350 UTC, the organization of the lee wave pattern had decreased considerably in the WRF model output (Fig. 8).

Init: 0000 UTC Mon 09 Jan 17 Fcst: 23.83 h
 Valid: 2350 UTC Mon 09 Jan 17 (1650 MST Mon 09 Jan 17)
 Vertical velocity XY= 302.0,333.0 to 455.0,333.0
 Potential temperature XY= 302.0,333.0 to 455.0,333.0

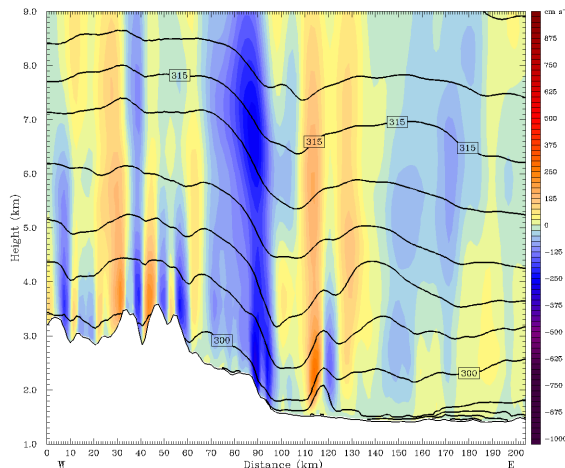


Figure 8: As in Fig. 6 except time is 2350 UTC. The lee wave pattern has weakened since the time shown in Fig. 6 (2050 UTC).

The actual evolution of the wave echo during this same general time period was monitored by the execution of continuous, two sweep RHI scans with the CSU-CHILL radar between 2110 and 2306 UTC. The upward sweep was done on an azimuth of 285°; the downward sweep azimuth was 290°. This scan sequence repeated at time intervals of 2 minutes and 8 seconds. Over the course of these RHI

observations, the Bragg echo wave pattern remained fairly stationary until approximately 2200 UTC. After that time, the echo layer pattern began to fluctuate more rapidly. A “braided” echo pattern containing localized, enhanced reflectivity curls also began to appear (Fig. 9). The development of small scale curls has been observed during the turbulent breakdown of waves that developed in stable layers in the coastal Virginia area (Fig. 10; Hicks and Angell, 1968). The Bragg echo enhancement that occurs during the wave breakdown has been ascribed to an increase in C_n^2 as the turbulent air motions increase the refractive index variations on the half radar wavelength scale.

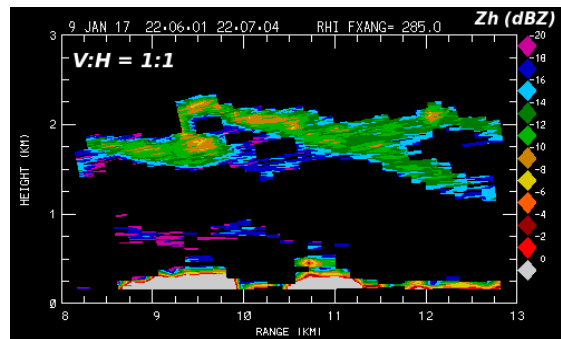


Figure 9: Reflectivity data in a 285° RHI scan at 2206 UTC. Small scale curl and braid structures associated with wave breakdown are visible.

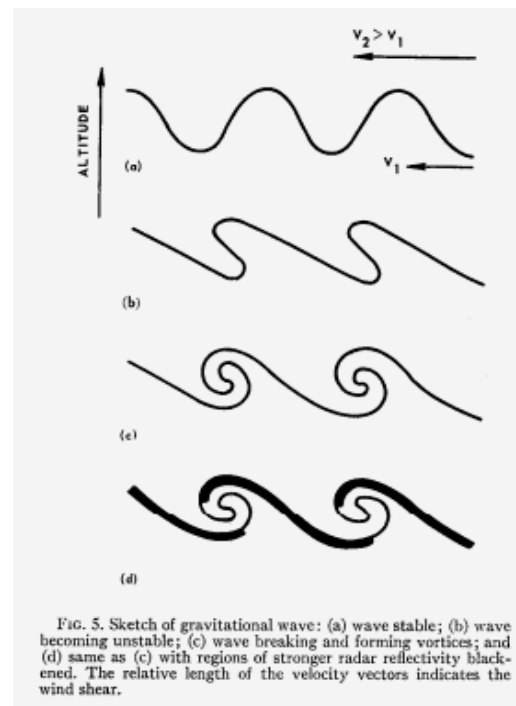


FIG. 5. Sketch of gravitational wave: (a) wave stable; (b) wave becoming unstable; (c) wave breaking and forming vortices; and (d) same as (c) with regions of stronger radar reflectivity blackened. The relative length of the velocity vectors indicates the wind shear.

Figure 10: Schematic of gravitational wave breakdown process. From Fig. 5 of Hicks and Angell (1968)

4. Conclusions

S-band radar's capabilities for the detection of Bragg scattering echoes from precipitation-free areas have been demonstrated over the past several decades. Initial interest was in understanding the source of "angel echoes" (Hardy and Katz, 1969). Recently, more practical applications for Bragg scattering layers have been developed, notably mapping of mesoscale variability in the boundary layer of the tropical oceanic atmosphere (Davison et al., 2013), and characterizing the stability of the differential reflectivity calibrations in the WSR-88D radar network. (Richardson et al., 2017).

The results of the current study indicate that Bragg echo observations can also be useful in monitoring the characteristics and evolution of topographically-generated lee waves. While this basic capability was demonstrated through received power measurements in the early 1970's (Starr and Browning, 1972), more modern radar technology allows the routine collection of high resolution observations including a wider variety of measurements (i.e. radial velocity and dual polarization data). These observations can provide useful verification data for numerical models of lee waves. Comparisons of pilot reports of turbulence with Bragg echo wave signatures are also worthy of exploration. To these ends, the collection of additional CSU-CHILL radar data sets during future periods of lee wave activity will be done.

Acknowledgements:

The CSU-CHILL national radar facility is supported by: NSF AGS-1460585

References:

- Davison, J.L., R.M. Rauber, and L. Di Girolamo, 2013: A revised conceptual model of the tropical marine boundary layer. Part II: Detecting relative humidity layers using Bragg scattering from S-Band radar. *J. Atmos. Sci.*, **70**, 3025-3046.
- Hardy, K.R. and I. Katz, 1969: Probing the clear Atmosphere with high power, high resolution radars. *Proc. IEEE*, **57**, 468-480.
- Hicks, J.J, and J.K. Angell, 1968: Radar observations of breaking gravitational waves in the visually clear atmosphere. *J. Appl. Meteor*, **7**, 114-121.
- Knight, C.A. and L.J. Miller, 1993: First radar echoes from cumulus clouds. *Bull. Amer. Meteor. Soc.*, **74**, 179-188.

Melnikov, V.M., R.J. Doviak, D.S. Zrnic, and D.J. Stensrud, 2011: Mapping Bragg scatter with a polarimetric WSR-88D. *J. Atmos. And Oceanic Tech*, **28** 1273-1285.

Richardson, L.M., J. Cunningham, W.D. Zittel, R.R. Lee, R.L. Ice, V. Melnikov, N. Hoban, and J.G. Gebauer, 2017: Bragg scattering detection by the WSR-88D. Part I: Algorithm development. *J. Atmos. and Oceanic. Tech*, **34** 465-478.

Scorer, R.S., 1949: Theory of waves in the lee of mountains. *QJRMS* **75**, 41-56

Starr, J.R. and K.A. Browning, 1972: Observations of lee waves by high-power radar. *QJRMS*, **94**, 73-85.